



ORIGINAL RESEARCH

A xenograft study of human adipose stromal cell-based vocal fold mucosal replacement in rabbits

Eric K. Tran MD¹  | Yazeed Alhiyari PhD¹ | Kevin Juarez MD^{1,2} |
Bhavani Shankara Gowda PhD^{1,3} | Feng Schrader BA^{1,3} | Dipti P. Sajed MD, PhD⁴ |
Jennifer L. Long MD, PhD^{1,3} 

¹Department of Head and Neck Surgery, David Geffen School of Medicine at University of California, Los Angeles, Los Angeles, California, USA

²Department of Anesthesiology and Perioperative Care, University of California-San Francisco Health, San Francisco, California, USA

³Greater Los Angeles Veterans Affairs Healthcare System, Los Angeles, California, USA

⁴Department of Pathology and Laboratory Medicine, Los Angeles, David Geffen School of Medicine at University of California, Los Angeles, California, USA

Correspondence

Jennifer L. Long, Department of Head and Neck Surgery, David Geffen School of Medicine at UCLA, 650 Charles Young Drive, CHS room 62-132, Los Angeles, CA 90095, USA.

Email: jlong@mednet.ucla.edu

Funding information

NIH National Center for Advancing Translational Sciences (NCATS), Grant/Award Number: UL1TR001881; National Institutes of Health, Grant/Award Number: NIDCD R01 DC016959; UCLA Jonsson Comprehensive Cancer Center; Department of Veteran Affairs, Greater Los Angeles VA Healthcare System

[Correction added on Oct 8, 2022, after first online publication: Acknowledgment section have been added in this version]

Abstract

Objectives: Vocal fold (VF) scarring, manifested by increased collagen, decreased glycosaminoglycans (GAGs), and disrupted elastic fibers, remains a negative consequence of VF injury or resection. The objective of this study is to compare four reconstructive options after VF mucosal resection in rabbits. A Cell-Based Outer Vocal fold Replacement (COVR) using human adipose-derived mesenchymal stromal cells (hASCs) in fibrin scaffold is directly compared with a decellularized scaffold implant, hASC injection, and resection alone without reconstruction. The primary hypothesis is that the cells-in-scaffold construct better reconstitutes the VF structure than either cells or scaffold alone, or than healing by secondary intention.

Methods: A total of 49 rabbits received bilateral VF cordectomy, followed by either COVR implant, decellularized scaffold implant, hASC injection, or no reconstruction (injured control group). Larynges were harvested after 6 weeks.

Results: Histology demonstrated greater lamina propria thickness, less collagen deposition, and more GAGs in COVR animals versus all other treatment groups. Evidence of persistent human cells was found in about half of the cell-treated animals. RNA levels of fibrosis pathway and macrophage phenotype markers were statistically unchanged among treatment groups at 6 weeks.

Conclusion: These data support the efficacy of COVR implantation in restoring VF microstructure in rabbits. The intact COVR was required; isolated components of decellularized scaffold or injected hASC still produced histologic scarring. We propose that the unique bilayered cell structure within fibrin enables controlled matrix remodeling to minimize wound contraction and fibrosis, and to promote GAG deposition.

Level of Evidence: Basic science study

KEYWORDS

adipose-derived stromal cells, decellularized scaffold, extracellular matrix, fibrin, regenerative medicine, vocal fold

This is an open access article under the terms of the [Creative Commons Attribution-NonCommercial-NoDerivs](https://creativecommons.org/licenses/by-nc-nd/4.0/) License, which permits use and distribution in any medium, provided the original work is properly cited, the use is non-commercial and no modifications or adaptations are made.

© 2022 The Authors. *Laryngoscope Investigative Otolaryngology* published by Wiley Periodicals LLC on behalf of The Triological Society.

1 | INTRODUCTION

Vocal fold (VF) mucosa consists of epithelium overlying a specialized lamina propria (LP) not found elsewhere in the body. Its unique microstructure, with an extracellular matrix (ECM) comprised of layered elastic fibers, basket-weave collagen, and interspersed hyaluronic acid (HA), confers specific viscoelastic properties allowing vibration to produce voice. Injury, often due to resection or irradiation for treatment of head and neck cancers or other masses, leads to scarring and fibrosis that replaces functional tissue with dense collagen, rendering the ECM stiff and difficult to phonate. Current treatments are suboptimal and generally do not address the pathological ECM.¹⁻⁵ More radical approaches are needed, particularly for moderate-to-severe cases of scarring in which normal ECM may not be restored by injectable therapies alone.

Regenerative medicine in the form of cell-based therapy represents a potentially more powerful treatment, by introducing new cells capable of restoring damaged or lost tissue. Implanted cells can respond to host signaling to continually adapt throughout time, mediating regeneration and abrogating new scar formation via improved wound healing. This differs from traditional pharmaceutical or growth factor therapy, which acts through narrower mechanisms and does not adapt to host signaling. The simplest form of regenerative medicine is directly injecting cells into the VF. Although three different types of autologous cell injections have been studied in clinical trials, the results have been mixed with inadequate response in cases of severe scarring, indicating the continued need to develop additional therapeutic options.¹⁻⁴

Another option would be to remove dysfunctional VF mucosa and replace it with new tissue. In order to restore normal phonatory vibration, such a VF replacement must heal without scarring. This limits the utility of mucosal transplant from donor VFs, which do experience ECM alteration during the healing process.⁵ Our group has therefore developed a cell-based graft resembling the true VF in gross architecture and mechanical stiffness, termed the Cell-based Outer Vocal fold Replacement (COVR). The COVR is composed of adipose-derived mesenchymal stromal cells (ASC) suspended in a fibrin matrix. Differentiation of ASC in a polarized fashion with air interface and epidermal growth factor (EGF) exposure leads to a multilayered structure with epithelial and mesenchymal cells, resembling the VF epithelium, and LP that it aims to replace.⁶ We hypothesize that the unique bilayered differentiation of these cells within the supportive niche provided by the fibrin scaffold allow the COVR to incorporate into surrounding tissue with minimal fibrosis and pathologic inflammation. The end result is a hybrid tissue cohabited by host and implant cells, which communicate to produce orderly ECM remodeling. In an immunocompetent rabbit model, COVR produced with allogeneic rabbit ASC produced better functional outcomes at 4 weeks than VF autotransplant, despite a simpler initial microstructure.⁷

This study aims to determine whether the ASC, the wound coverage with complex ECM, or the unique combination of both within the COVR is primarily responsible for the improved VF healing that was observed in pilot studies. The COVR implant is compared directly versus human ASC (hASC) injection, decellularized COVR gel, and injured control after bilateral VF cordectomy in rabbits. Human cells are used

in this immunocompetent xenograft experiment to better predict the behavior of a human therapy. Initial mechanistic exploration investigates macrophage and fibrosis pathways as potential mediators of wound healing in this system.

2 | MATERIALS AND METHODS

2.1 | In vitro culture and gel fabrication

Culture conditions are as previously described.⁶ Briefly, hASC (from American Type Culture Collection) were expanded under standard conditions. Cells were authenticated and verified by flow cytometry for ASC markers, directed mesenchymal differentiation assay, and independent laboratory polymerase chain reaction (PCR) testing to exclude human viruses and contaminating cell lines.

COVR implants were formed from hASC, rabbit fibrinogen (Innovative Research), and bovine thrombin (Sigma-Aldrich) at a 4:1:1 ratio, as shown in Figure 1. A total of 600,000 cells were supplied in each 600 μ l COVR gel, to approximate the cell density in VF LP. Solutions were mixed in 12-mm Transwell (Corning) inserts and incubated at 37°C; gelation occurred within 30 min. Differentiation medium containing 10 ng/ml human recombinant EGF (Promega Corp) was supplied at the basal surface. After 2 weeks in culture, COVR was harvested by incising and peeling the Transwell membrane from the insert and gel while maintaining its orientation. Resultant COVR constructs were cylindrical, 12 mm in diameter, and 2-mm to 3-mm thick. Each COVR was cut in half with a scalpel to apply to the two injured VFs per rabbit.

Decellularized constructs (Decell) were formed by transferring mature COVR gels within the Transwell inserts into sterile 0.1% sodium dodecyl sulfate (SDS) solution (Figure 1). Gels were continuously rocked for 3 days, with daily change of the SDS solution, followed by phosphate-buffered saline (PBS) wash for 1 day before implantation. Resulting Decell constructs were similar in size to COVR. 4',6-diamidino-2-phenylindole (DAPI) stain confirmed absence of cell nuclei. Extra COVR and Decell samples underwent rapid gram stain confirming no bacterial contamination prior to implantation. Two Decell gels and two COVR gels were subjected to uniaxial tensile testing with the Bose ElectroForce tensile testing system as previously described for VFs to compare their mechanical properties.⁸

hASC destined for VF injection were harvested immediately prior to surgery. 600,000 cells were prepared in 0.4 ml of PBS and stored in a capped syringe on ice until ready for injection. Each VF received half the amount, or 300,000 cells. For control animals, 0.4 ml of sterile PBS was prepared in an injection syringe.

2.2 | Animal treatments

All activities were approved by the Institutional Animal Care and Use Committee, following United States Department of Agriculture guidelines. A total of 49 male New Zealand white rabbits were randomly assigned to postcordectomy treatment groups: COVR implant,

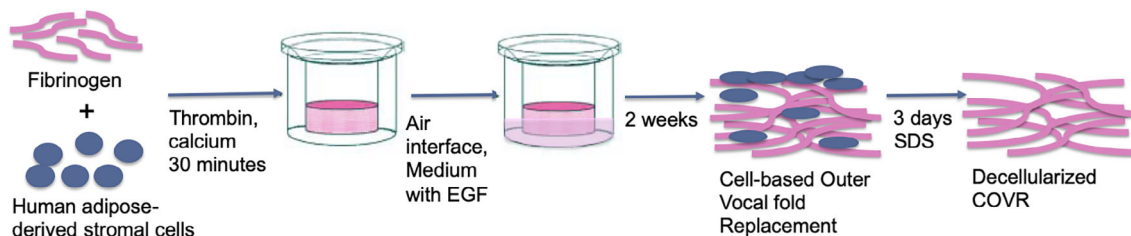


FIGURE 1 Schematic drawing of implant fabrication. Fibrinogen and human adipose-derived mesenchymal stromal cells are combined, with addition of thrombin and calcium, to form a Cell-Based Outer Vocal fold Replacement (COVR) gel within the insert of a Transwell cell culture insert. Cell culture medium containing epidermal growth factor (EGF) is then supplied to the base of the insert, leaving an air interface at the top of the gel. After 2 weeks, COVR is either harvested for use, or treated with sodium dodecyl sulfate (SDS) for 3 days for decellularization.

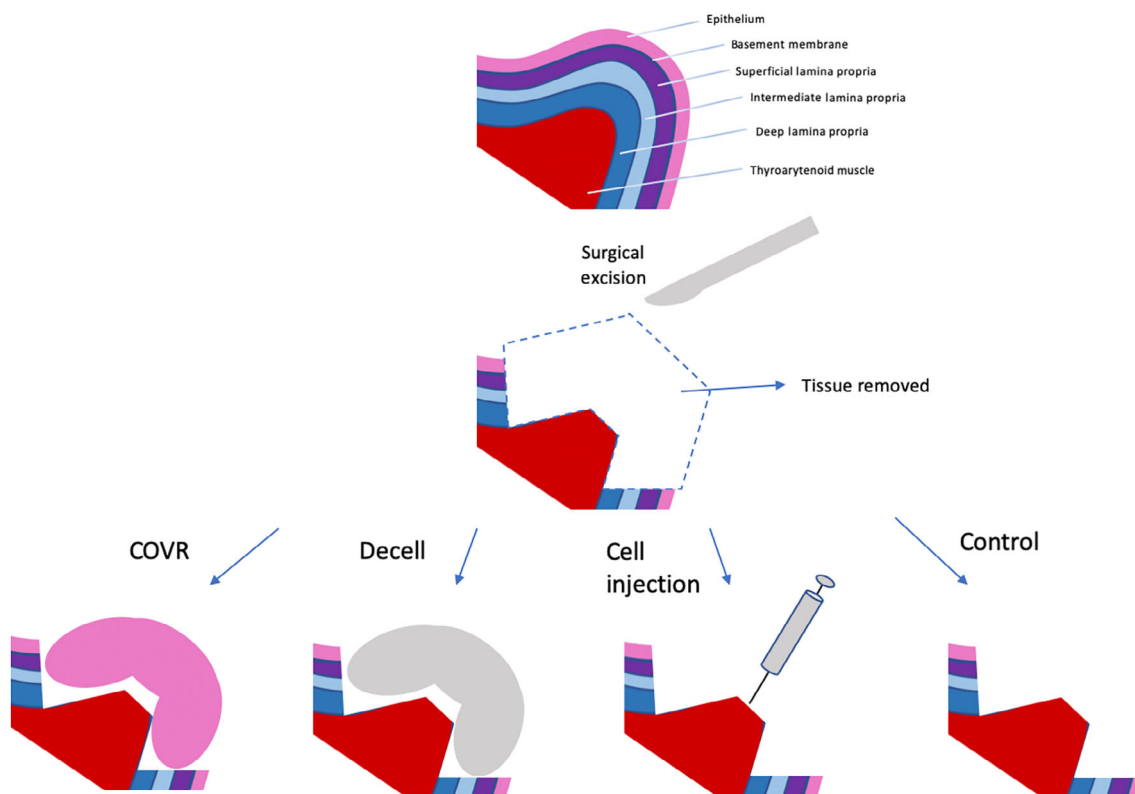


FIGURE 2 Schematic drawing of surgical interventions. Vocal fold is drawn in coronal cross-section to demonstrate the epithelium, lamina propria, and thyroarytenoid muscle layers. All animals underwent surgical removal of all the mucosal layers, along the entire length of the membranous vocal fold. The four reconstruction methods are shown: Cell-Based Outer Vocal fold Replacement (COVR) implant, decell implant, cell injection into remaining vocal fold muscle, and control without reconstruction

decellularized implant, hASC injection, or control (no reconstruction; Figure 2). Surgery was performed through a vertical neck incision. A temporary tracheotomy provided airway management during surgery. Midline laryngofissure opened the thyroid cartilage, exposing the VFs. Bilateral vibratory VF mucosae were resected by sharp dissection from the anterior commissure to the arytenoid cartilage, exposing thyroarytenoid muscle. Reconstruction then proceeded according to treatment group. For the COVR and Decell groups, gels were positioned with air-liquid interface oriented towards the laryngeal lumen and were sutured to underlying muscle. The cell injection group had 300,000 cells injected directly into each thyroarytenoid muscle in 0.2 ml of sterile PBS. The control group received bilateral injection of 0.2 ml of sterile

PBS. Wounds were closed after careful hemostasis. Postoperatively all rabbits received buprenorphine for analgesia and dexamethasone to reduce laryngeal swelling for 3 days, and antibiotics and famotidine for 10 days. Animals were euthanized with intravenous pentobarbital, 6 weeks after surgeries. Larynges were harvested and processed immediately.

2.3 | Larynx microscopy

After excision, larynges were dissected to focus on the surgical site. A 2 mm segment of VF mucosal tissue at the area of implantation was

Group	COVR	hASC	Decell	Control
n (number of rabbits analyzed)	12	11	12	12
Mean LP thickness (μm)	785 \pm 222*	531 \pm 257	511 \pm 217	434 \pm 194
Dense collagen (%)	0	73	67	58
GAGs (%)	83	55	33	50
Elastin fibers (%)	25	18	17	8
Elastin clumps (%)	0	27	25	17
Fibrin (%)	17	0	50	8
Leukocytic infiltrate (any, %)	58	64	50	17
Intense infiltrate or abscess (%)	25	45	33	0
HLA positive (% immunocytochemical)	58	55	0	0
HLA positive (% western)	45	27	0	0

TABLE 1 Results by treatment group at 6 weeks

Note: “%” indicates percent of animals with this finding. * $p < .05$ one-way ANOVA versus control. Abbreviations: COVR, Cell-Based Outer Vocal fold Replacement; GAGs, glycosaminoglycans; hASC, human adipose-derived mesenchymal stromal cells; HLA, human leukocyte antigen; LP, lamina propria.

biopsied for western blot and real-time quantitative PCR. VFs were then formalin-fixed, paraffin-embedded, and sectioned in an axial plane. Each larynx underwent hematoxylin and eosin (H&E) and Movat's pentachrome stains, and immunohistochemistry for human leukocyte antigen (HLA). Movat's pentachrome delineates ECM components using Alcian blue to detect glycosaminoglycans (GAGs), ferric chloride with phosphotungstic acid for elastic fibers, saffron yellow for collagen, and crocein scarlet-acid fuchsin for muscle.

Histology slides were reviewed in a blinded fashion by a clinical pathologist (Dipti P. Sajed) and the primary surgeon (Jennifer L. Long). Collagen, GAGs, elastin, and acellular fibrin were qualitatively assessed on Pentachrome stain. Leukocytic infiltrate was assessed at high power on H&E sections, and was rated as none, any, or intense infiltrate/abscess if a discrete collection of leukocytes was noted.

Maximum width of the LP was measured using EVOS XL Core Cell Imaging System at low magnification. Two sections from each animal were viewed, one stained with H&E and one with Pentachrome stain. A total of four VFs were thus examined for each animal. LP was identified and measured as a line perpendicular from the epithelial basement membrane to the thyroarytenoid muscle, at either 4 \times or 10 \times magnification. The thickest point of each VF LP was manually measured on the digital display, and converted to actual microns using the integrated scale bar. Regions containing abundant glands or fat were avoided, as indicators of a false VF location. Regions with heavy leukocyte infiltrate were also avoided since these exhibit greater thickness. Some VFs were not measured due to sectioning artifact or lack of any VF in the plane of sectioning. A total of 42 animals had measurement of between one and four VFs. The mean value of maximal LP thickness was calculated for each animal. Group means and standard deviations were calculated and presented in Table 1.

Immunohistochemistry for HLA used a monoclonal primary antibody formed against a fusion protein containing human HLA-A, B, and C epitopes (Monoclonal HLA-66013, ThermoFisher Scientific). Antigen retrieval was performed with 10 mM sodium citrate for 40 min at

95 degrees. 10% goat serum for 30 min blocked nonspecific binding sites. Primary antibody (1:5000 in 1% bovine serum albumin [BSA]) was incubated for 1 h at 37°C then overnight at 4°C. Negative control slides were incubated with 1% BSA alone, without HLA antibody. After washing, secondary antibody (goat antimouse IgG labeled with fluorophore 633) was applied at room temperature for 2 h. Slides were washed and coverslipped with Vecta-Shield aqueous mounting agent with DAPI, and viewed within 48 h. Immunohistochemistry was performed three times per rabbit, to assess for consistency of results. Labeling was classified as absent, present, or indeterminate. HLA was classified as “indeterminate” if the labeled cells were very sparse, were inconsistent among the three staining trials for each animal, or were difficult to distinguish from BSA-labeled negative controls.

2.4 | Molecular analysis

Biopsy specimens were kept frozen at -80°C until use, then divided for western blot and PCR. Western blotting was performed as a second method to detect HLA protein, using the same monoclonal antibody as above. Samples were homogenized in SDS sample solution, boiled to denature, and run in polyacrylamide gel electrophoresis. Proteins were transferred onto membrane for blotting. Anti-HLA primary antibody was used at 1:2000, with goat antimouse IgG labeled with horseradish peroxidase as secondary antibody at 1:3000. Chemiluminescence was developed with enhanced chemiluminescence substrate on film.

For quantitative PCR, gene-specific primers were designed for rabbit mRNA sequences for CD80, CD163, nuclear receptor subfamily 4 group A member 1, and suppressor of mothers against decapentaplegic homolog 3 (**CD80**: F-TCACAAGGTCTCACCTAAATTTGC, R-AGACGCTTTCTGCA-GAGTCA. **CD163**: F-CCAAAGACAGTGTCTGTTGCC, R-TGTCATCACAGATGGTGCC. **NR4A1**: F-CACATTGCCAGGAAGAGCCCC, R-TTGATACAGGGCATCTCGGC. **Smad3**: F-TTTGGCCCTGCTTCGAG-GAC, R-GTTGAGCCGGACATCCCAC). A rabbit GAPDH primer was used for housekeeping gene. Quantitative real-time reverse transcriptase

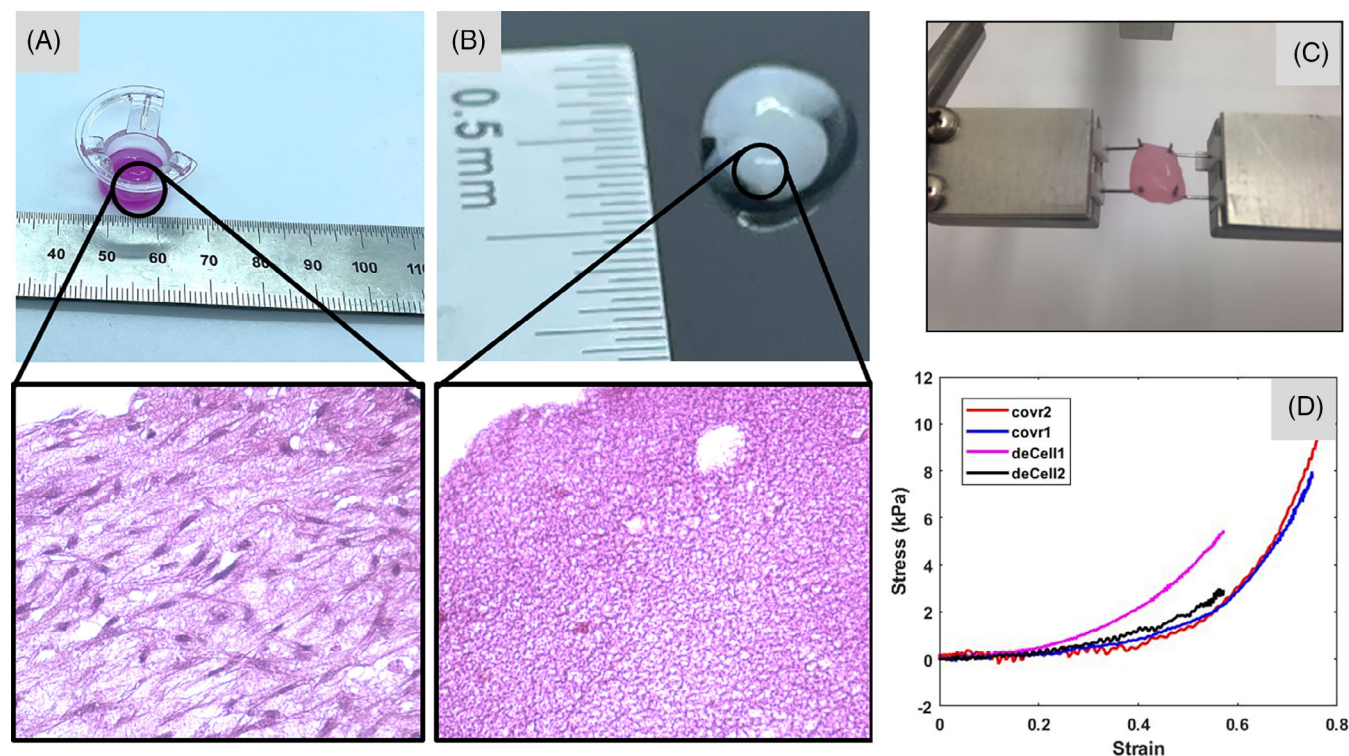


FIGURE 3 Comparison of Cell-Based Outer Vocal fold Replacement (COVR) and decell gels. (A) COVR implant formed within Transwell cell culture insert. Figure inset shows 4× Movat's pentachrome stain demonstrating scattered cell nuclei within fibrin scaffold. (B) Decell implant formed by sodium dodecyl sulfate treatment of COVR implant. Figure inset shows absence of cell nuclei on histology, 4×. (C) COVR gel mounted for uniaxial tensile testing with a Bose ElectroForce testing system. (D) Stress–strain curves for two COVR and two decell gels, showing similar mechanical behavior among the four gels tested

PCR was run on equal amounts of RNA from each specimen using QuantiTect SYBR Green RT-PCR kit (Qiagen), for analysis with the $\Delta\Delta Ct$ method. Delta Ct was calculated as the cycle threshold difference between each gene result and the sample's corresponding GAPDH result; triplicate samples were averaged to determine the sample mean. Mean ΔCt was calculated for the normal VF group. Delta delta Ct was then calculated for each experimental sample and gene by subtracting the normal mean ΔCt from the experimental sample ΔCt . Group mean $\Delta\Delta Ct$ and standard deviation were calculated for each gene by combining individual animals' results within each treatment group. Fold change from normal was calculated as 2 to the power of negative $\Delta\Delta Ct$. For statistical analysis, a one-way analysis of variance (ANOVA) with Dunnett's post hoc analysis was performed on all the treatment groups ANOVA (Injured control, Cell injection, COVR implant, Decell implant). A p -value $< .05$ was considered statistically significant.

3 | RESULTS

3.1 | COVR and Decell fabrication and mechanics

Figure 3 shows examples of COVR and Decell implants. Stress–strain curves from uniaxial tensile testing show similar mechanical behavior among the four gels tested.

3.2 | Perioperative course

Of the 49 immunocompetent male rabbits that underwent laryngofissure and bilateral VF cordectomy, two died prematurely. One (Control group) died in the immediate perioperative period from adverse Ketamine reaction, and one (COVR group) died on postoperative Day 2 from solid food aspiration. Both deaths were considered unrelated to the treatment group. Subsequent animals were not given Ketamine and were fed only soft diet for 2 days postop. The remaining 47 animals all gained weight and survived to planned euthanasia and larynx harvest at 6 weeks. Some animals exhibited noisy breathing postoperatively, that was monitored and typically resolved within a few days.

Histologic features from the two animals with perioperative deaths are shown in Figure 4. Figure 4A demonstrates complete VF mucosa resection, with removal of all epithelium and LP at Day 0 in the control group. Figure 4B shows successful grafting of the COVR at Day 2, with close adherence to the thyroarytenoid muscle.

3.3 | Wound healing

Wound healing at 6 weeks postsurgery was evaluated using H&E and Movat's Pentachrome staining (Figure 5 and Table 1). Many injured

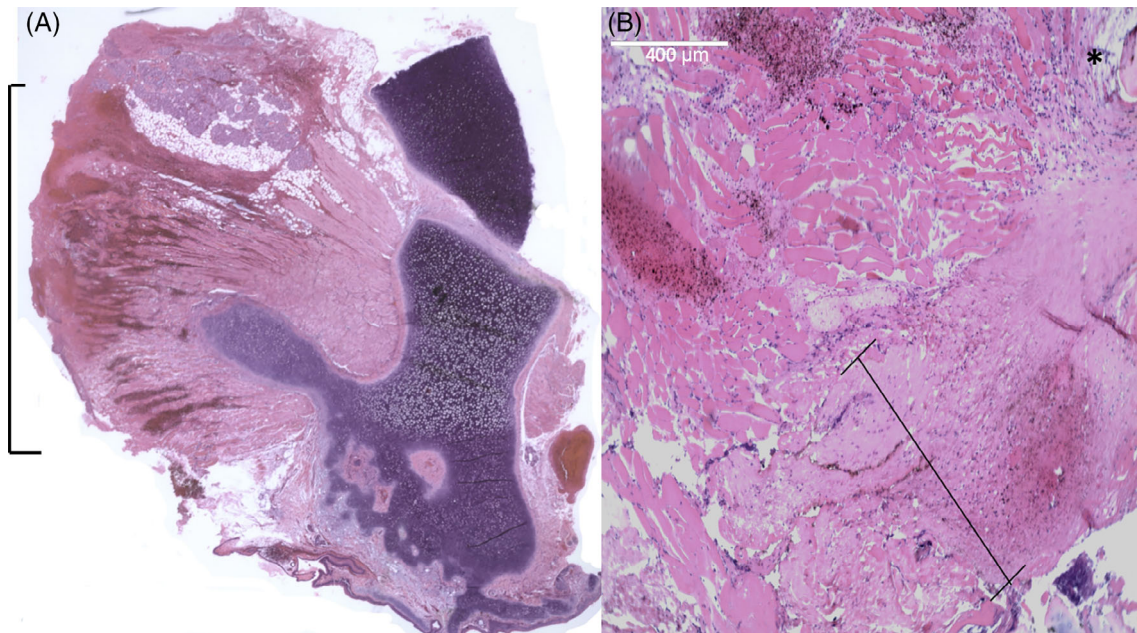


FIGURE 4 Early postoperative histology in rabbit hemilarynges. (A) Control group, postoperative Day 0 after medication-related death. Bracket demonstrates region of vocal fold (VF) mucosa resection with removal of all epithelium and lamina propria from the true VF, and blood collected within residual thyroarytenoid muscle. The thyroid cartilage was removed during specimen processing and appears as a cut edge at the top of the image, adjacent to glands and fat from the paraglottic space. Arytenoid cartilage is seen at the bottom of the image. (B) Comparison of Cell-Based Outer Vocal fold Replacement (COVR) group, postoperative Day 2 after death from aspiration. Bracket demonstrates the width of the COVR implant overlying the thyroarytenoid muscle. A suture is cut in cross-section at the top right corner (*)

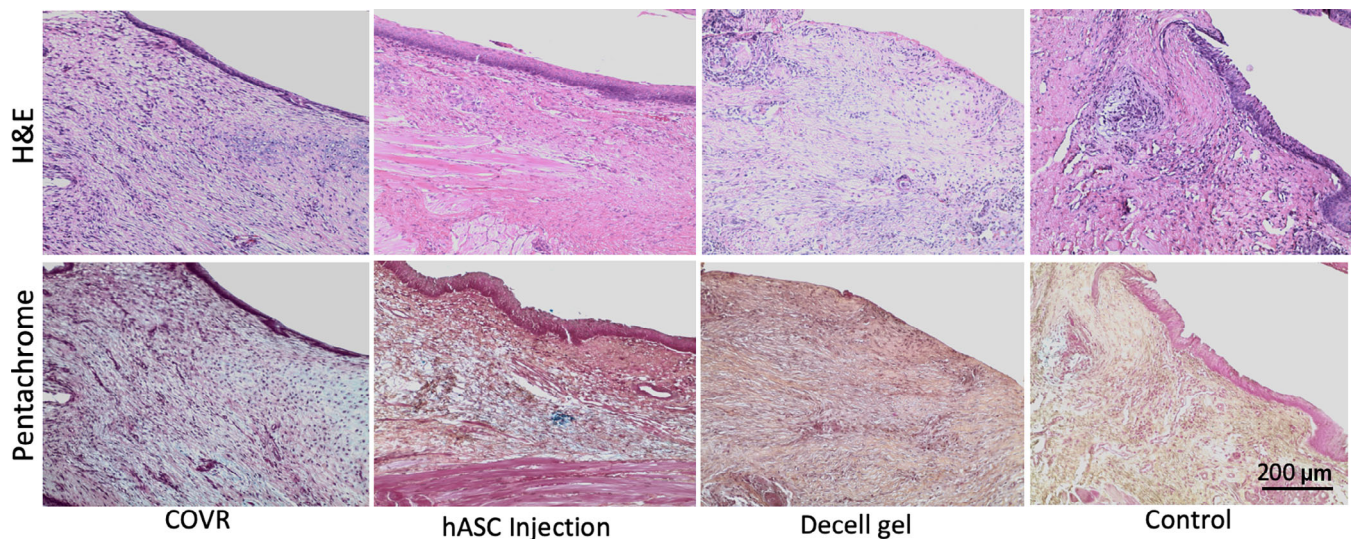


FIGURE 5 Lamina propria histology, 20 \times . Representative examples for each group at 6 weeks postsurgery are shown. Top row is standard H&E stain; bottom row is Movat Pentachrome stain showing elastic fibers in black, collagen in yellow-brown, muscle, and epithelium in magenta, glycosaminoglycan (GAG) in blue. From left to right: Comparison of Cell-Based Outer Vocal fold Replacement (COVR) group shows minimal collagen deposition and GAGs dispersed throughout (blue color on Pentachrome stain). Lamina propria is thick, with the thyroarytenoid muscle out of this field of view. Human adipose-derived mesenchymal stromal cells injection group shows thin lamina propria, dense collagen deposition (yellow-brown color on Pentachrome) and minimal GAGs. Decell group demonstrates collagen deposition throughout, scattered persistent fibrin seen as acellular eosinophilic regions on H&E stain, incomplete epithelialization, and no GAGs. Control group shows collagen deposition, complete epithelialization, and no GAGs. Elastic fibers are not seen in any of these examples

control VFs had thin or absent LP, with epithelium nearly overlying thyroarytenoid muscle. COVR specimens exhibited the widest LP, the greatest degree of GAGs, and the least prominent collagen of

any group. Injection, Decell, and Control groups all showed prominent dense collagen and only scattered presence of GAGs. Residual fibrin was most prominent in the Decell group, with only occasional

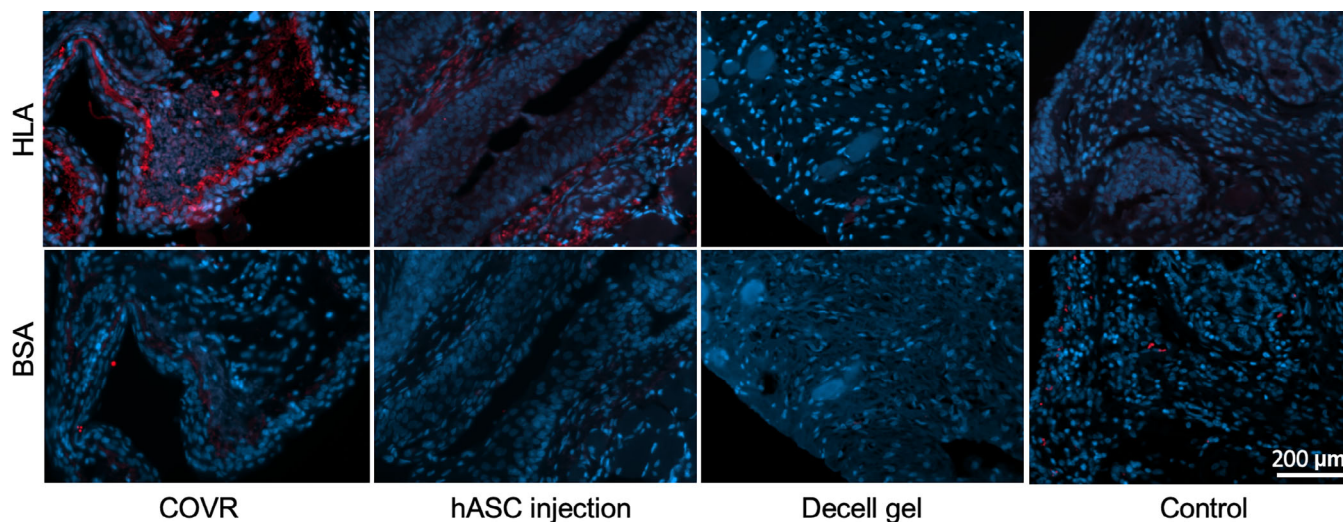


FIGURE 6 Immunohistochemistry for HLA. Representative images are shown for each group at 20X. Cell nuclei appear blue, and secondary antibody labeling appears red. Top row shows HLA antibody, bottom row shows BSA negative control without primary antibody. About half of the animals receiving cells exhibited positive staining similar to these examples. BSA, bovine serum albumin; COVR, Comparison of Cell-Based Outer Vocal fold Replacement; HLA, human leukocyte antigen, hASC, human adipose-derived mesenchymal stromal cells.

small areas consistent with fibrin or resolving hematoma in the other groups. Normal-appearing fine elastic fibers were only occasionally observed in any group but were most prominent in COVR specimens. The COVR group did not have clumpy, thickened elastic fibers that were occasionally present in all other groups. Leukocytic infiltrate was present to varying degrees, as indicated in Table 1. Few control animals had any leukocytes noted, while all three implanted groups had leukocytes identified in over half of animals and the greatest amount in hASC injections.

3.4 | HLA expression

Presence of HLA was assessed with immunohistochemical (IHC) labeling by an antibody to the conserved region of HLA groups A, B, and C (Figure 6). COVR and hASC groups had clearly and consistently detectable HLA in 7 of 12 (58%, COVR) and 6 of 11 (55%, hASC) animals examined after 6 weeks (Table 1). One animal from each group had no identifiable labeling; the remaining animals were considered indeterminate based on scant or inconsistent labeling. Decell implant and injured control animals showed no HLA labeling. COVR implants consistently exhibited stronger or more widespread HLA labeling than hASC injections did. HLA-positive cells in the COVR implants were found in the epithelium and LP layers and were interspersed with HLA-negative cells presumed to be host rabbit cells. In the hASC-injected larynges, HLA-positive cells were typically identified within the LP but not the epithelium, and sometimes had a linear pattern that suggested a needle track. Western blotting confirmed HLA protein in 45% of COVR samples and 27% of cell injection samples (Figure 7).

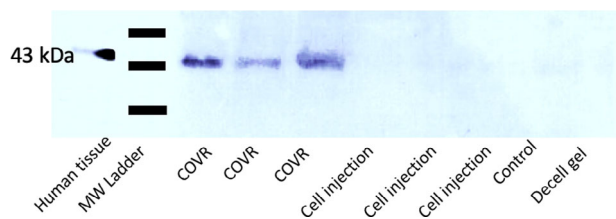


FIGURE 7 Western blot for human leukocyte antigen (HLA). An example blot containing samples from each group is shown, with bands identified at 43 kDa as expected for HLA. Positive samples in this blot are the human tissue positive control, and all three Comparison of Cell-Based Outer Vocal fold Replacement (COVR) samples tested. HLA was not detected in the cell injection samples on this blot, nor in the control and decell samples which did not receive human cells

3.5 | Gene expression

Quantitative RT-PCR was used to compare selected RNA expression levels from all animals at 6 weeks after VF resection and treatment (Figure 8). Results are presented as fold change versus expression levels in normal rabbit VFs from unoperated animals.

Transcription factors NR4A1 and SMAD3, both involved in VF wound healing and fibrosis, were measured. NR4A1 expression was downregulated in all groups, most notably in hASC injections. SMAD3 expression was similar in all groups to normal VF, with <2-fold change. No findings differed statistically from injured control, at a *p*-value of .05.

Macrophage-associated genes CD80 and CD163 both increased modestly in all operated groups relative to normal VFs, but none of the treatment groups differed statistically from injured control.

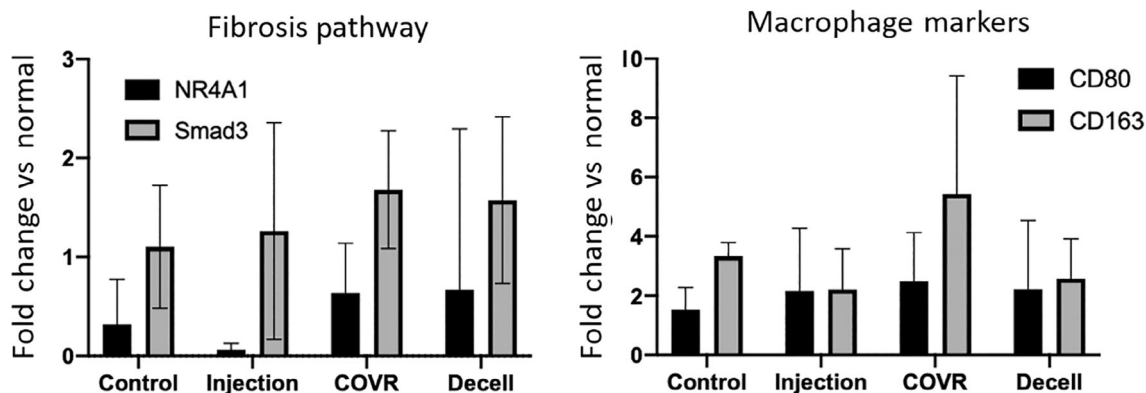


FIGURE 8 Quantitative RT-PCR of fibrosis pathway mediators NR4A1 and SMAD3 and macrophage markers CD80 and CD163. Fold change of RNA expression is shown for the four treatment groups, relative to unoperated normal rabbit vocal folds. Bars show mean of all animals in the treatment group ($n = 11$ or 12 each), and error bars show SD. Each sample was run in triplicate. In the left panel, NR4A1 was reduced from normal in all groups; differences were not statistically significant versus control. SMAD3 was unchanged from normal in all groups. In the right panel, both macrophage markers were increased from normal in all groups, but treatment groups did not differ from control. COVR, Cell-Based Outer Vocal fold Replacement

4 | DISCUSSION

VF scarring remains a difficult problem to treat due to disruption of the unique LP that is necessary for normal voicing. Current therapies have limited ability to restore the characteristic microstructure, and recurrent scarring is a risk of any intervention. The goals of tissue replacement are thus to restore functional LP while minimizing subsequent fibrosis. We previously showed that a tissue-engineered COVR with allogeneic rabbit ASC-reduced collagen deposition and improved tissue vibration relative to resection alone or autotransplant of intact VF mucosa.⁷ This study further proposes that the unique combination of ASC organized within the mature fibrin scaffold is critical for implant success, rather than individualized components of cells or scaffold alone. We also update the COVR itself to use hASC, which is a necessary preclinical step to prepare for human translation.

4.1 | COVR implantation improves VF ECM

Histologically, COVR-implanted larynges demonstrated the best restoration of LP structure with less dense collagen and prominent GAGs. Elastic fibers, while rare, were the closest to normal appearance in COVR VF without thickened clumps. In contrast, VF in both the cell injection and Decell groups demonstrated findings similar to scarred controls, with thin LP, prominent collagen, and infrequent GAGs.

Markedly increased GAGs was a hallmark of the COVR animals in this study. GAGs, especially HA, are essential proteoglycans in healthy VF that maintain fluidity during the high-frequency collisions of voicing.⁹ Loss of HA is a well-known characteristic of VF scarring. Potential pathways for the increased GAGs found in COVR-treated animals include induction of HA synthase expression, inhibition of degradation, or more efficient integration into the fibrin ECM; this study did not directly examine these mechanisms.

Successful ECM restoration in this study was found primarily in the COVR group, in which a cellular neo-mucosa was implanted. The decellularized scaffold alone did not restore normal ECM, instead producing excess collagen and very little GAGs. Residual acellular fibrin was prominent in half of Decell implants at 6 weeks, indicating poor incorporation into native tissue. Similar results have been described for decellularized tissue implant for glottic reconstruction.¹⁰

Injecting undifferentiated hASC alone did not restore LP width, and did not protect the injured VF from excess collagen deposition during recovery. This finding contrasts with prior MSC injection studies in rabbits.^{11,12} Differences between this study and other reports include a greater cell number injected (here, 300,000 cells per rabbit VF vs. 80,000–100,000), lack of immunosuppression, and injection via laryngofissure after LP resection instead of endoscopic injury. Note that this study was designed to most closely compare the influence of hASC alone versus hASC within the COVR implant, so results may not be directly comparable to other cell injection schema. The findings do indicate that in the setting of immunocompetent VF reconstruction, the benefits of the three-dimensional implant are not conferred by the cellular component alone.

Comparison between differentiated and undifferentiated ASC within fibrin scaffold was not performed and could be a focus of future study to determine if the neo-epithelium offers specific benefit beyond merely serving as a supportive scaffold for undifferentiated cells. If similar benefits can be achieved, the manufacturing process could be simplified. Additionally, this work assessed results at 6 weeks only, which is relatively early in the timecourse of VF wound healing.

4.2 | Human cell persistence at 6 weeks after xenogeneic VF implantation

Human cells were implanted into immunocompetent rabbits in this study, in contrast to previous work which implanted rabbit-derived

ASC.¹³⁻¹⁵ This shift was undertaken to better demonstrate the efficacy of eventual human therapy, as is recommended by the FDA for preclinical work in preparation for clinical trials.¹⁶ Also, since human use will likely use autologous cells without immunosuppression, no immunosuppression was administered in this experiment. Some inflammatory response was therefore expected and was indeed noted in all reconstructed groups, including the decellularized gel.

About half of animals receiving human cells by injection or COVR implant still had some cells with detectable HLA by immunohistochemistry after 6 weeks. Human cells with HLA expression were interspersed with cells not expressing HLA, presumed to be host rabbit cells that migrated into the wound area (Figure 6). These results were similar to our previous study of four female rabbits that received male rabbit ASC within a COVR implant.¹⁵ All four of those rabbits had a mixture of implanted and host cells after 4 weeks, based on *in situ* hybridization for the rabbit Y chromosome. In this study, the epithelium was seen to have a mixture of implant and host cells in the COVR group only; the hASC group was re-epithelialized with exclusively host cells. No rabbit in either group had a majority of cells expressing HLA.

Western blot detected HLA protein in fewer animals, especially in the hASC Injection group (Table 1). The lower HLA detection rate in Western blot may have occurred due to partial VF sampling which could miss cells that were not well dispersed geographically. Nonspecific staining on IHC is another possibility, but stringent criteria for assessing IHC images make this less likely. It is also possible that the hASC downregulated their expression of HLA, thus evading detection by Western blot and IHC. RT-PCR was attempted to clarify the data at a genomic level, but was found to be unreliable due to nonspecific human primer recognition of rabbit tissues. Similar findings regarding partial persistence of implanted cells have been described in prior literature, especially at this early timepoint.^{12,17,18}

Although implanted cells do not engraft long-term, their initial presence within the implanted scaffold is critical. Implanting decellularized gel led to suboptimal results with fibrotic LP, possibly due to lack of hASC. We hypothesize that hASC play a necessary role in matrix remodeling, inhibiting fibroblast migration, and preventing scar contracture during early wound healing. However, hASC injected alone without the scaffold also resulted in fibrotic LP. This underscores the complex effects of the COVR implant that are not reproduced by its individual components. The fibrin scaffold may provide a protective niche which supports hASC survival and better enables the hASC to exert paracrine influence on surrounding fibroblasts.¹⁹ The scaffold also concentrates cells and their emitted products within the area of interest to better guide wound healing.

4.3 | Mechanistic pathway normalization by 6 weeks postinjury

The fibrosis pathway in this system was assessed by measuring messenger RNA for the nuclear receptor NR4A1 and the signaling

molecule SMAD3. NR4A1 is thought to be anti-fibrotic early after injury and SMAD3 is upregulated in fibrotic wound healing pathways. In rats, NR4A1 is induced by transforming growth factor-beta-1 (TGF- β 1) after VF injury, peaking around Day 7 then declining to near normal by Day 30.²⁰ Conversely at 6 weeks in our rabbit model, NR4A1 expression was downregulated in all groups versus normal. All reconstruction groups (hASC Injection, COVR, and Decell) were statistically unchanged from injured control. SMAD3 is a profibrotic mediator that is also upregulated by TGF- β 1; in rabbits it also has been found to peak at 7 days after injury then return to normal by 30 days.²¹ Similarly, SMAD3 expression here was near normal in all groups including injured control at 6 weeks. An earlier time-course study with direct measurement of TGF- β 1, SMAD3, and NR4A1 proteins could better identify any relevant changes in this signaling pathway after VF reconstruction.

Another facet in the complex VF wound healing process is the macrophage activation state. CD80 and CD163 gene expression were assessed as indicators of M1 (proinflammatory) and M2 (anti-inflammatory/tissue remodeling) phenotypes, respectively.²² We hypothesized that favorable wound healing results would correlate with greater M2 macrophage activity. However, our data did not demonstrate statistically significant difference in macrophage activation state among experimental groups at this 6-week timepoint. Both CD80 and CD163 expression increased modestly in all groups relative to normal VFs, as expected due to macrophage influx after injury. Multiparametric flow cytometry is a better method to assess macrophage phenotypes but requires a larger amount of fresh tissue. Previous flow cytometry in pigs after VF injury also found no difference in macrophage phenotype at 3 or 7 days among hydrogel with allogeneic porcine ASC, hydrogel injection alone, and injured control.²³

Alternate mechanistic pathways can be considered for further evaluation. Fibroblast phenotype was not assessed here and is a key driver of fibrotic versus reparative state. Also, the presence of immature epithelium in the COVR implant distinguishes it from the other groups studied, and may be a key factor underlying improved wound healing. Further study of epithelial signaling, and prevention of epithelial-mesenchymal transformation in the host cells, may provide mechanistic insights.

4.4 | Limitations

Some limitations of this work must be considered. All results were assessed at 6 weeks, which was selected as a single mid-range timepoint. Earlier examination may better demonstrate mechanistic pathway differences, while later examination is required to show ultimate wound healing and cell fate. Functional and biomechanical outcomes were not considered here, and are best studied for a longer time period. Histologic assessments are qualitative and subject to variability based on location. Histologic comparisons were not made directly to normal VFs, but to injured controls. Thus, the most similar clinical application is reconstruction after VF resection, which is limited to severe cases of scarring or mucosal disease.

4.5 | Conclusions

This study in rabbits demonstrates that a COVR more effectively reconstructs the three-dimensional VF mucosa after resection than either its cellular or scaffold components alone. Findings at 6 weeks include lessened collagen deposition, more GAGs, and absence of elastin clumps in COVR-treated animals relative to injured controls; those outcomes were not found with either cell injection or decellularized scaffold reconstruction. We propose that the unique implant of human adipose-derived stromal cells, differentiated within fibrin hydrogel to a bilayered epithelial and mesenchymal structure, enables rapid VF tissue reconstruction without inducing scar contracture and fibrosis. Further work will continue translating this therapy by assessing functional voice restoration, long-term ECM outcomes, and mechanistic study focusing on epithelial and fibroblastic signaling.

ACKNOWLEDGEMENT

We gratefully acknowledge the contribution of Dr. Zhaoyan Zhang, who conducted uniaxial tensile testing.

AUTHOR CONTRIBUTIONS

Eric K. Tran: Collection and/or assembly of data, data analysis and interpretation, article writing. **Yazeed Alhiyari:** Collection and/or assembly of data, data analysis and interpretation, article writing, administrative support. **Kevin Juarez:** Collection and/or assembly of data, data analysis and interpretation, and article writing. **Feng Xu Schrader:** Administrative support, collection and/or assembly of data, and data analysis and interpretation. **Bhavani Gowda:** Collection and/or assembly of data and data analysis and interpretation. **Dipti P. Sajed:** Data analysis and interpretation. **Jennifer L. Long:** Conception and design, data analysis and interpretation, article writing, and final approval of article.

FUNDING INFORMATION

This work was supported by the National Institutes of Health, NIDCD R01 DC016959 (Jennifer L. Long). Additional support provided by: Department of Veteran Affairs, Greater Los Angeles VA Healthcare System; UCLA Jonsson Comprehensive Cancer Center; and NIH National Center for Advancing Translational Science (NCATS) UCLA CTSI Grant Number UL1TR001881.

CONFLICT OF INTEREST

The authors declare that there is no conflict of interest that could be perceived as prejudicing the impartiality of the research reported.

ORCID

Eric K. Tran  <https://orcid.org/0000-0003-4506-9266>

Jennifer L. Long  <https://orcid.org/0000-0002-4185-2328>

REFERENCES

- Mattei A, Bertrand B, Jouve E, et al. Feasibility of first injection of autologous adipose tissue-derived stromal vascular fraction in human scarred vocal folds: a nonrandomized controlled trial. *JAMA Otolaryngol Head Neck Surg.* 2020;146(4):355-363. doi:10.1001/jamaoto.2019.4328
- Chhetri DK, Berke GS. Injection of cultured autologous fibroblasts for human vocal fold scars. *Laryngoscope.* 2011;121(4):785-792. doi:10.1002/lary.21417
- Ma Y, Long J, Amin MR, et al. Autologous fibroblasts for vocal scars and age-related atrophy: a randomized clinical trial. *Laryngoscope.* 2020;130(11):2650-2658. doi:10.1002/lary.28453
- Nagubothu SR, Sugars RV, Tudzarovski N, et al. Mesenchymal stromal cells modulate tissue repair responses within the injured vocal fold. *Laryngoscope.* 2020;130(1):E21-E29. doi:10.1002/lary.27885
- Long J, Salinas J, Rafizadeh S, Luegmair G, Zhang Z, Chhetri D. In vivo vocal fold cover layer replacement. *Laryngoscope.* 2015;125(2):406-411. doi:10.1002/lary.24924
- Long JL, Zuk P, Berke GS, Chhetri DK. Epithelial differentiation of adipose-derived stem cells for laryngeal tissue engineering. *Laryngoscope.* 2010;120(1):125-131. doi:10.1002/lary.20719
- Long JL. Repairing the vibratory vocal fold. *Laryngoscope.* 2018;128(1):153-159. doi:10.1002/lary.26801
- Zhang Z, Samajder H, Long JL. Biaxial mechanical properties of human vocal fold cover under vocal fold elongation. *J Acoust Soc Am.* 2017;142(4):EL356. doi:10.1121/1.5006205
- Gray SD, Titze IR, Chan R, Hammond TH. Vocal fold proteoglycans and their influence on biomechanics. *Laryngoscope.* 1999;109(6):845-854. doi:10.1097/00005537-199906000-00001
- Kitamura M, Hirano S, Kanemaru SI, et al. Glottic regeneration with a tissue-engineering technique, using acellular extracellular matrix scaffold in a canine model. *J Tissue Eng Regen Med.* 2016;10(10):825-832. doi:10.1002/term.1855
- Hertegard S, Cedervall J, Svensson B, et al. Viscoelastic and histologic properties in scarred rabbit vocal folds after mesenchymal stem cell injection. *Laryngoscope.* 2006;116(7):1248-1254. doi:10.1097/01.mlg.0000224548.68499.35
- Kim YM, Yi T, Choi JS, et al. Bone marrow-derived clonal mesenchymal stem cells as a source of cell therapy for promoting vocal fold wound healing. *Ann Otol Rhinol Laryngol.* 2013;122(2):121-130. doi:10.1177/000348941312200208
- Morisaki T, Kishimoto Y, Tateya I, et al. Adipose-derived mesenchymal stromal cells prevented rat vocal fold scarring. *Laryngoscope.* 2018;128(1):E33-E40. doi:10.1002/lary.26855
- Shiba TL, Hardy J, Luegmair G, Zhang Z, Long JL. Tissue-engineered vocal fold mucosa implantation in rabbits. *Otolaryngol Head Neck Surg.* 2016;154(4):679-688. doi:10.1177/0194599816628501
- Goel AN, Gowda BS, Veena MS, Shiba TL, Long JL. Adipose-derived mesenchymal stromal cells persist in tissue-engineered vocal fold replacement in rabbits. *Ann Otol Rhinol Laryngol.* 2018;127(12):962-968. doi:10.1177/0003489418806008
- USDA. *Preclinical assessment of investigational cellular and gene therapy products.* USDA. 2019. Accessed June 1, 2021.
- Choi JW, Park JK, Chang JW, et al. Small intestine submucosa and mesenchymal stem cells composite gel for scarless vocal fold regeneration. *Biomaterials.* 2014;35(18):4911-4918. doi:10.1016/j.biomaterials.2014.03.008
- Svensson B, Nagubothu SR, Nord C, et al. Stem cell therapy in injured vocal folds: a three-month xenograft analysis of human embryonic stem cells. *Biomed Res Int.* 2015;2015:754876. doi:10.1155/2015/754876
- Whelan D, Caplice NM, Clover AJ. Fibrin as a delivery system in wound healing tissue engineering applications. *J Control Release.* 2014;196:1-8. doi:10.1016/j.jconrel.2014.09.023
- Hiwatashi N, Bing R, Kraja I, Branski RC. NR4A1 is an endogenous inhibitor of vocal fold fibrosis. *Laryngoscope.* 2017;127(9):E317-E323. doi:10.1002/lary.26678
- Hiwatashi N, Benedict PA, Dion GR, et al. SMAD3 expression and regulation of fibroplasia in vocal fold injury. *Laryngoscope.* 2017;127(9):E308-E316. doi:10.1002/lary.26648

22. Orecchioni M, Ghosheh Y, Pramod AB, Ley K. Macrophage polarization: different gene signatures in M1(LPS+) vs. classically and M2(LPS-) vs alternatively activated macrophages. *Front Immunol.* 2019;10:1084. doi:[10.3389/fimmu.2019.01084](https://doi.org/10.3389/fimmu.2019.01084)
23. King SN, Woo JH, Tang S, Thibeault SL. Macrophage response to allogeneic adipose tissue-derived stromal cells in Hyaluronan-based hydrogel in a porcine vocal fold injury model. *Ann Otol Rhinol Laryngol.* 2017;126(6):463-477. doi:[10.1177/0003489417702923](https://doi.org/10.1177/0003489417702923)

How to cite this article: Tran EK, Alhiyari Y, Juarez K, et al. A xenograft study of human adipose stromal cell-based vocal fold mucosal replacement in rabbits. *Laryngoscope Investigative Otolaryngology.* 2022;7(5):1521-1531. doi:[10.1002/lio2.929](https://doi.org/10.1002/lio2.929)